A NEW NON-ITERATIVE RECONSTRUCTION METHOD FOR THE ELECTRICAL IMPEDANCE TOMOGRAPHY PROBLEM

A. D. FERREIRA AND A. A. NOVOTNY

Abstract. The electrical impedance tomography (EIT) problem consists in determining the distribution of the electrical conductivity of a medium subject to a set of current fluxes, from measurements of the corresponding electrical potentials on its boundary. EIT is probably the most studied inverse problem since the fundamental works by Calderón from the eighties. It has many relevant applications in medicine (detection of tumors), geophysics (localization of mineral deposits) and engineering (detection of corrosion in structures). In this work, we are interested in reconstructing a number of anomalies with different electrical conductivity from the background. Since the EIT problem is written in the form of an overdetermined boundary value problem, the idea is to rewrite it as a topology optimization problem. In particular, a shape functional measuring the misfit between the boundary measurements and the electrical potentials obtained from the model is minimized with respect to a set of ball-shaped anomalies by using the concept of topological derivatives. It means that the objective functional is expanded and then truncated up to the second order term, leading to a quadratic and strictly convex form with respect to the parameters under consideration. Thus, a trivial optimization step leads to a non-iterative second order reconstruction algorithm. As a result, the reconstruction process becomes very robust with respect to noisy data and independent of any initial guess. Finally, in order to show the effectiveness of the devised reconstruction algorithm, some numerical experiments into two spatial dimensions are presented, taking into account total and partial boundary measurements.

1. Introduction

A wide class of inverse problems can be written in the form of overdetermined boundary value problems. Such a difficult can be overcome by rewriting the inverse problem in the form of an optimization problem. The basic idea consists in minimizing an objective functional measuring the misfit between a given data and a numerical solution with respect to the parameters under consideration. In particular, let us consider a geometrical domain Ω with its boundary denoted as $\Gamma = \partial\Omega$. A boundary value problem is defined in Ω, whose solution is denoted by u^*. We assume that the response of the system on the boundary Γ can be observed. For example, given a Dirichlet data U on Γ, the associated Dirichlet-to-Neumann map for a second order elliptic equation is defined as follows [8]

$$\Lambda_{\omega^*} \ : \ u^* = U \mapsto Q := \partial_n u^* \quad \text{on} \quad \Gamma.$$

where ω^* is an unknown set of anomalies embedded within Ω and n is the exterior unit normal vector on Γ. Therefore, given the pair (U, Q) we want to reconstruct the set $\omega^* \subset \Omega$. The mathematical model of the system furnishes the mapping $\omega \mapsto \Lambda_\omega$ for a family of anomalies ω. Thus, taking U we can generate the output of the model $\Lambda_\omega(U)$ and compare it with the given function $Q = \Lambda_{\omega^*}(U)$. Hence, using the mathematical model we can consider the associated optimization problem based on the distance minimization between the observation (U, Q) and the model response $(U, \Lambda_\omega(U))$ over the family of admissible anomalies ω.

In this paper the Electrical Impedance Tomography (EIT) is adopted as model problem, which consists in finding the number, size, shape and location of a set of hidden anomalies inside a body from total or partial measurements of the electrical potential on the boundary of the body.

Since the unknown of the problem we are dealing with is given by a geometrical domain ω^* representing the set of hidden anomalies, then it can be written in the form of a topology optimization problem. Thus, the topological derivative concept is used [26], which can be

Key words and phrases. EIT problem, new reconstruction algorithm, topological asymptotic expansion, topological derivatives.

seen as a particular case of the broader class of asymptotic methods fully developed in the books by Ammari & Kang [4] and Ammari et al. [2], for instance. See also related works [22, 23, 24, 25]. In the context of EIT problem, important contributions can be found in [6, 10, 11, 12, 16, 17, 18]. The stability and resolution analysis for a (first-order) topological derivative based imaging functional in the context of Helmholtz equation is known [3]. However, such an analysis is missing for the conductivity problem we are dealing with. Therefore, the second-order topological derivative concept starts to play an important role in the context of the inverse conductivity problem. In particular, it has been successfully applied for solving a class of EIT problem in [7, 13]. In the paper [7] a higher order expansion of a tracking-type shape functional with respect to a number of arbitrary shaped inclusion is derived, all of them controled by the same small parameter. The resulting expansion is used to reconstruct a single circular or elliptical inclusion from partial boundary measurement. In [13] a second-order topological expansions of a tracking-type shape functional is also considered with respect to several circular inclusions of uniform sizes. The resulting expansion is used to initialize a standard level set method.

In our approach the anomalies are approximated by a finite number of ball-shaped trial inclusions of different sizes. In addition, we have evoked the adjoint method *a posteriori*, after obtaining the associated sensitivities, allowing us to derive a simpler representation for the resulting expansion. These two ingredients were crucial in the development of the proposed novel reconstruction algorithm, which represents the main contribution of our paper with respect to [7, 13]. In particular, following the original ideas presented in [9], the objective functional is expanded and then truncated up to the second order term, leading to a quadratic and strictly convex form with respect to the parameters under consideration. Finally, a trivial optimization step leads to a non-iterative second order reconstruction algorithm. As a result, the reconstruction process becomes very robust with respect to noisy data and independent of any initial guess, allowing us to approximate the topology as well the shape of the hidden anomalies through a number of trial balls. Therefore, our approach can be used either as a standalone tool to accurately and quickly detect a set of hidden anomalies, even with several connected components, or as an initialization for more complex iterative approaches such as the ones based on level-sets methods [15, 19], for instance.

The paper is organized as follows. In Section 2 the mathematical formulation of the inverse EIT problem is introduced and rewritten as a topological optimization problem. In Section 3 the second order topological expansion of the shape functional is presented. The novel non-iterative reconstruction algorithm is devised in Section 4. Some reconstruction experiments from total and partial boundary measurements are presented in Section 5. Finally, in Section 6 the paper ends with some concluding remarks.

2. The Inverse Conductivity Problem

Let us consider a domain $\Omega \subset \mathbb{R}^2$ with Lipschitz continuous boundary $\partial\Omega$. The domain Ω represents a body endowed with the capability of conducting electricity. Its electrical conductivity coefficient is denoted by $k^*(x) \geqslant k_0 > 0$, with $x \in \Omega$ and $k_0 \in \mathbb{R}_+$. If the body Ω is subjected to a given electric flux Q on $\partial\Omega$, then the resulting electric potential u in Ω is observed on a part of the boundary $\Gamma_m \subset \partial\Omega$. The objective is to reconstruct the electrical conductivity k^* over Ω from a given boundary measurement $u^*_{|\Gamma_m} = U$, solution of the following overdetermined boundary value problem

$$\left\{\begin{array}{rcll} \operatorname{div}[q(u^*)] & = & 0 & \text{in } \Omega, \\ q(u^*) & = & -k^*\nabla u^*, & \\ q(u^*)\cdot n & = & Q & \text{on } \partial\Omega, \\ u^* & = & U & \text{on } \Gamma_m. \end{array}\right. \tag{2.1}$$

Without loss of generality, we are considering only one boundary measurement U on Γ_m. The extension to several boundary measurements is trivial.

An important feature of the human body is that the electrical conductivity can be approximated by a piecewise constant function representing different tissues. The electrical conductivity of the muscles, lungs, bones and blood are respectively given by 8.0, 1.0, 0.06 and 6.7 milisiemens (mS), for instance. Thus, we assume that the unknown electrical conductivity k^* we are looking for belongs to the following set

$$C_\gamma(\Omega) := \left\{ \varphi \in L^\infty(\Omega) : \varphi = k \left(\mathbb{1}_\Omega - \sum_{i=1}^{N} (1-\gamma_i)\mathbb{1}_{\omega_i} \right) \right\}, \tag{2.2}$$

where $k \in \mathbb{R}_+$ is the electrical conductivity of the background. When the conductivity k depends on the frequency, see [1]. The sets $\omega_i \subset \Omega$, with $i = 1, \cdots, N$, are such that $\omega_i \cap \omega_j = \emptyset$, for $i \neq j$. In addition, $\mathbb{1}_\Omega$ and $\mathbb{1}_{\omega_i}$ are used to denote the characteristics functions of Ω and ω_i, respectively. Finally, $\gamma_i \in \mathbb{R}_+$ are the contrasts with respect to the electrical conductivity of the background k. From these elements, the inverse problem we are dealing with can be stated as:

Problem 1. *Let $Q \in H^{-1/2}(\partial\Omega)$ be a given Neumann excitation, then find $k^* \in C_\gamma(\Omega)$ from observations of the field U on $\Gamma_m \subset \partial\Omega$, such that $u^*[k^*] \in H^1(\Omega)$ satisfies (2.1).*

We assume that each ω_i is measurable and simply connected. We also assume that the values of the electrical conductivity of the background k and the associated contrasts γ_i are known (see counter-example at the end of this section). From these assumptions, Problem 1 can be written as a topology optimization problem with respect to the sets ω_i, for $i = 1, \cdots, N$. In fact, let us introduce the unknown set $\omega^* = \bigcup_{i=1}^{N^*} \omega_i^* \subset \Omega$, where N^* is the number of anomalies we are looking for. Therefore

$$k^*(x) = \begin{cases} k & \text{if } x \in \Omega \setminus \omega^*, \\ \gamma_i k & \text{if } x \in \omega_i^*,\ i = 1, \cdots, N^*. \end{cases} \tag{2.3}$$

See sketch in Figure 1(a). Now, let us introduce the following auxiliary Neumann boundary value problem: Find u, such that

$$\begin{cases} \operatorname{div}[q(u)] &= 0 & \text{in } \Omega, \\ q(u) &= -k_\omega \nabla u, & \\ q(u)\cdot n &= Q & \text{on } \partial\Omega, \\ \int_{\partial\Omega} Q &= 0, & \\ \int_{\Gamma_m} u &= \int_{\Gamma_m} U, & \end{cases} \tag{2.4}$$

where Q and U are the boundary excitation and boundary measurement, respectively and $k_\omega \in C_\gamma(\Omega)$ is constant by parts, characterized by a set $\omega \subset \Omega$. See sketch in Figure 1(b).

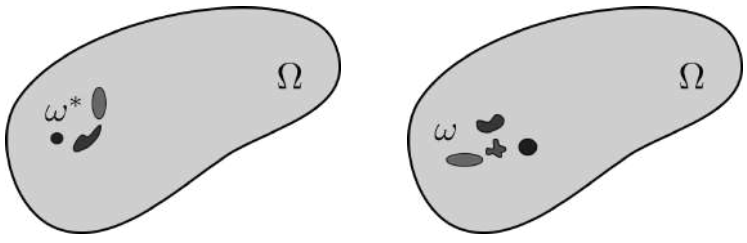

(a) ω^* (b) ω

FIGURE 1. A body Ω with a set of anomalies.

Finally, we introduce the following shape functional measuring the misfit between the boundary measurement U and the solution $u = u(\omega)$ of (2.4) evaluated on Γ_m, namely

$$\mathcal{J}_\omega(u) = \int_{\Gamma_m} (u - U)^2. \tag{2.5}$$

Since the electrical conductivity of the background k and the associated contrasts γ_i are known by assumption, then solving Problem 1 is equivalent to solve the following topology optimization problem with respect to the support ω of the anomalies

$$\underset{\omega\subset\Omega}{\text{Minimize}}\ \mathcal{J}_\omega(u), \quad \text{subject to (2.4)}. \tag{2.6}$$

The problem of finding $k^* \in C_\gamma(\Omega)$ for a given Dirichlet excitation U on $\partial\Omega$, from observations of the flux Q on $\Gamma_m \subset \partial\Omega$, by using similar optimization approach can be found in [5].

Remark 2. *In the case of the EIT problem in general a number M of boundary measurements is available, which are easily obtained by combining different pairs of injection and draining electrodes. See sketch in Figure 4, for instance. However, for the sake of simplicity and without lost of generality, in this paper all derivations are presented by taking into account just one single boundary measurement. Their extensions for a number $M > 1$ of measurements is trivially obtained after sum-up the sensitivities associated with each individual boundary measurement.*

The minimization problem (2.6) we are dealing with is based on the following paradigm: we know what we are looking for, but we do not know where they are. In fact, we cannot reconstruct both the topology ω^* and the contrasts γ_i, $i = 1, \cdots, N^*$. Let us present a simple counter-example. It consists of an inclusion of radius ρ and contrast γ centered into a disk of unity radius with electrical conductivity $k = 1$. We introduce a polar coordinate system (r, θ) at the center of the inclusion. The disk is excited with an electric flux $Q = \sin(\theta)$ applied on its boundary. The solution $u = u(r, \theta)$ of problem (2.4), evaluated on the boundary of the disk, is given by $u(1, \theta) = \beta \sin(\theta)$, with

$$\beta = \frac{(1+\gamma) + \rho^2(1-\gamma)}{(1+\gamma) - \rho^2(1-\gamma)}. \tag{2.7}$$

For a fixed pair (ρ^*, γ^*), the boundary measurement is given by $U = \beta^* \sin(\theta)$. After solving the minimization problem (2.6), we can write γ as a function of ρ, namely

$$\gamma(\rho) = \frac{(1+\beta^*)\rho^2 + (1-\beta^*)}{(1+\beta^*)\rho^2 - (1-\beta^*)}. \tag{2.8}$$

By setting $\rho^* = 0.2$ and after taking the limit cases $\gamma^* \to 0$, $\gamma^* \to 1$ and $\gamma^* \to \infty$, the plot of $\gamma(\rho)$ with respect to ρ is shown in Figure 2, where we can observe the lack of uniqueness when both the radius ρ^* and the contrast γ^* are simultaneously unknown.

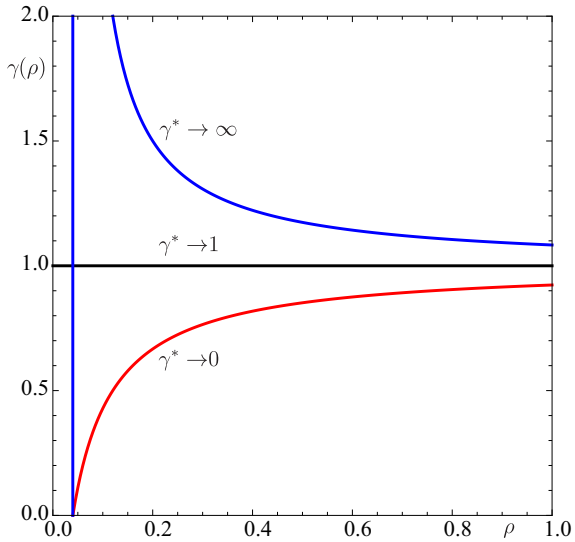

FIGURE 2. Counter-example of lack of uniqueness when both the topology and contrast are simultaneously unknown.

3. Topological Asymptotic Expansion

In this paper we deal with the reconstruction of $k^* \in C_\gamma(\Omega)$ from total or partial boundary measurement using the topological sensitivity analysis concept [26]. Therefore, let us consider $\omega = \emptyset$ and $u_0 = u_{|_{\omega=\emptyset}}$ solution of

$$\left\{\begin{array}{rcll} \operatorname{div}[q(u_0)] & = & 0 & \text{in } \Omega, \\ q(u_0) & = & -k\nabla u_0, & \\ q(u_0)\cdot n & = & Q & \text{on } \partial\Omega, \\ \int_{\partial\Omega} Q & = & 0, & \\ \int_{\Gamma_m} u_0 & = & \int_{\Gamma_m} U, & \end{array}\right. \tag{3.1}$$

where k is a constant that represents the electrical conductivity of the background. In this particular case, the following notation for the shape function is introduced

$$\mathcal{J}_0(u_0) = \int_{\Gamma_m} (u_0 - U)^2. \tag{3.2}$$

Let us perturb the domain Ω by nucleating – simultaneously – a number N of circular inclusions $B_{\varepsilon_i}(x_i)$ with contrast γ_i, $i = 1, \cdots, N$, as shown in Figure 3. We assume that $B_{\varepsilon_i}(x_i) \subset \Omega$ is a ball with center at $x_i \in \Omega$ and radius ε_i, such that $B_{\varepsilon_i}(x_i) \cap B_{\varepsilon_j}(x_j) = \emptyset$ for $i \neq j$. We introduce the notations $\xi = (x_1, \cdots, x_N)$ and $\varepsilon = (\varepsilon_1, \cdots, \varepsilon_N)$, whether necessary. The topologically perturbed counterpart of the shape functional is defined as follows

$$\mathcal{J}_\varepsilon(u_\varepsilon) = \int_{\Gamma_m} (u_\varepsilon - U)^2, \tag{3.3}$$

where u_ε is solution of the following boundary value problem

$$\left\{\begin{array}{rcll} \operatorname{div}[q_\varepsilon(u_\varepsilon)] & = & 0 & \text{in } \Omega, \\ q_\varepsilon(u_\varepsilon) & = & -\gamma_\varepsilon k\nabla u_\varepsilon, & \\ q_\varepsilon(u_\varepsilon)\cdot n & = & Q & \text{on } \partial\Omega, \\ \int_{\partial\Omega} Q & = & 0, & \\ \int_{\Gamma_m} u_\varepsilon & = & \int_{\Gamma_m} U, & \\ [\![u_\varepsilon]\!] & = & 0 & \text{on } \bigcup_{i=1}^N \partial B_{\varepsilon_i}(x_i), \\ [\![q_\varepsilon(u_\varepsilon)]\!]\cdot n & = & 0 & \text{on } \bigcup_{i=1}^N \partial B_{\varepsilon_i}(x_i), \end{array}\right. \tag{3.4}$$

with the contrast defined as

$$\gamma_\varepsilon = \gamma_\varepsilon(x) = \left\{\begin{array}{l} 1, \text{ if } x \in \Omega \setminus \bigcup_{i=1}^N B_{\varepsilon_i}(x_i) \\ \gamma_i, \text{ if } x \in B_{\varepsilon_i}(x_i). \end{array}\right. \tag{3.5}$$

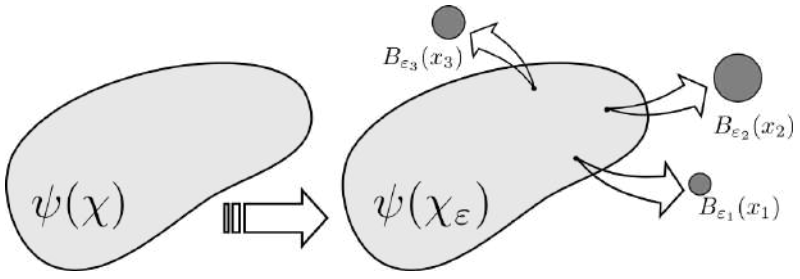

Figure 3. Perturbed domain representation.

3.1. **Asymptotic Expansion of the Solution.** General results for the asymptotic expansions of solutions in singularly perturbed domains were originally considered in [14, 21]. When perturbations are included in Ω, discrepancies over the inclusions $B_{\varepsilon_i}(x_i)$ in problem (3.1) appear.

The idea is to introduce boundary layers which compensate for such discrepancies. Thus, let us consider the following *ansätz* for the asymptotic expansion of u_ε

$$u_\varepsilon(x) = u_0(x) + \sum_{i=1}^{N} \left(w_i(x/\varepsilon_i) + \varepsilon_i^2 \tilde{u}_i(x) + \tilde{w}_i(x/\varepsilon_i) + \varepsilon_i^4 \tilde{\tilde{u}}_i(x) \right) + \sum_{i=1}^{N} \sum_{\substack{j=1 \\ j\neq i}}^{N} \left(w_i^j(x/\varepsilon_i) + \varepsilon_i^2 \varepsilon_j^2 u_i^j(x) \right) + \tilde{\tilde{u}}_\varepsilon(x). \quad (3.6)$$

Before continue, let us give a rough explanation of each term in the above expansion. The boundary layers w_i are introduced to compensate for the first and second order terms of the Taylor's expansion of ∇u_0 around x_i. The problem associate with $\tilde{u}_i$ compensates for the discrepancy introduced on $\partial\Omega$ by one term of w_i. The boundary layers $\tilde{w}_i$ compensate for the first and third term of the Taylor's expansion of $\nabla\tilde{u}_i$ and ∇u, respectively. There still discrepancies left on $\partial\Omega$ by one term of each set of boundary layers w_i and $\tilde{w}_i$, which are compensate by $\tilde{\tilde{u}}_i$. The terms w_i^j and u_i^j are introduced to take into account interactions between different inclusions. Finally, $\tilde{\tilde{u}}_\varepsilon$ compensate for all remainder discrepancies. Each term of the *ansätz* (3.6) are now explicitly defined. In what follows, the notation $\nabla^n\varphi(y)(x-x_i)^n$ represents the derivative of order n of a function φ in the direction $(x-x_i)$ evaluated at y.

We start with the boundary layers $w_i(x/\varepsilon_i)$, for $i = 1, \cdots, N$, which are solutions of

$$\begin{cases} \operatorname{div}[q_\varepsilon(w_i)] = 0 & \text{in } \Xi_\varepsilon, \\ q_\varepsilon(w_i) = -\gamma_{\varepsilon_i} k\nabla w_i & \text{in } \mathbb{R}^2, \\ w_i \to 0 & \text{at } \infty, \\ [\![w_i]\!] = 0 & \text{on } \partial B_{\varepsilon_i}(x_i), \\ [\![q_\varepsilon(w_i)]\!]\cdot n = k(1-\gamma_i)\left(\nabla u_0(x_i)\cdot n - \varepsilon_i \nabla^2 u_0(x_i) n\cdot n\right) & \text{on } \partial B_{\varepsilon_i}(x_i). \end{cases} \quad (3.7)$$

where $\Xi_\varepsilon := B_{\varepsilon_i}(x_i) \bigcup \left(\mathbb{R}^2 \setminus \overline{B_{\varepsilon_i}(x_i)}\right)$. By fixing the notation

$$\rho_i = \frac{1-\gamma_i}{1+\gamma_i} \quad \text{and} \quad \gamma_{\varepsilon_i} = \gamma_{\varepsilon_i}(x) = \begin{cases} 1, \text{ if } x \in \mathbb{R}^2 \setminus B_{\varepsilon_i}(x_i) \\ \gamma_i, \text{ if } x \in B_{\varepsilon_i}(x_i), \end{cases} \quad (3.8)$$

the solutions of (3.7) in $\mathbb{R}^2 \setminus \overline{B_{\varepsilon_i}(x_i)}$ are given by

$$w_i(x/\varepsilon_i) = \varepsilon_i^2 g_i(x) + \varepsilon_i^4 h_i(x), \quad (3.9)$$

where

$$g_i(x) = \frac{\rho_i}{\|x-x_i\|^2} \nabla u_0(x_i)\cdot(x-x_i) \quad (3.10)$$

and

$$h_i(x) = \frac{\rho_i}{2\|x-x_i\|^4} \nabla^2 u_0(x_i)(x-x_i)^2. \quad (3.11)$$

The functions $w_i^j(x/\varepsilon_j)$, $j \neq i$, satisfy

$$\begin{cases} \operatorname{div}[q_\varepsilon(w_i^j)] = 0 & \text{in } \Xi_\varepsilon, \\ q_\varepsilon(w_i^j) = -\gamma_{\varepsilon_j} k\nabla w_i^j & \text{in } \mathbb{R}^2, \\ w_i^j \to 0 & \text{at } \infty \\ [\![w_i^j]\!] = 0 & \text{on } \partial B_{\varepsilon_j}(x_j), \\ [\![q_\varepsilon(w_i^j)]\!]\cdot n_j = k(1-\gamma_j)\varepsilon_i^2 A_i(x_j)\nabla u_0(x_i)\cdot n_j & \text{on } \partial B_{\varepsilon_j}(x_j). \end{cases} \quad (3.12)$$

The second order tensor $A_i(x)$ is defined by

$$A_i(x) = \frac{\rho_i}{\|x-x_i\|^2}\left[I - 2\frac{(x-x_i)\otimes(x-x_i)}{\|x-x_i\|^2} \right]. \quad (3.13)$$

Thus, the solutions of (3.12) in $\mathbb{R}^2 \setminus \overline{B_{\varepsilon_j}(x_j)}$ are given by

$$w_i^j(x/\varepsilon_j) = \varepsilon_i^2 \varepsilon_j^2 \theta_i^j(x), \quad (3.14)$$

where

$$\theta_i^j(x) = \frac{\rho_i \rho_j}{\|x - x_j\|^2} A_i(x_j) \nabla u_0(x_i) \cdot (x - x_j). \tag{3.15}$$

Since the boundary layers w_i introduce discrepancies on $\partial\Omega$, we construct $\tilde{u}_i$, $i = 1, \cdots, N$, such that

$$\begin{cases} \operatorname{div}[q(\tilde{u}_i)] &= 0 & \text{in } \Omega, \\ q(\tilde{u}_i) &= -k\nabla\tilde{u}_i & \text{in } \Omega, \\ q(\tilde{u}_i)\cdot n &= -q(g_i)\cdot n & \text{on } \partial\Omega, \\ \int_{\Gamma_m} \tilde{u}_i &= -\int_{\Gamma_m} g_i, \end{cases} \tag{3.16}$$

where g_i is given by (3.10).

The boundary layers $\tilde{w}_i(x/\varepsilon_i)$, $i = 1, \cdots, N$, satisfy

$$\begin{cases} \operatorname{div}[q_\varepsilon(\tilde{w}_i)] &= 0 & \text{in } \Xi_\varepsilon, \\ q_\varepsilon(\tilde{w}_i) &= -\gamma_{\varepsilon_i} k\nabla\tilde{w}_i & \text{in } \mathbb{R}^2, \\ \tilde{w}_i &\to 0 & \text{at } \infty, \\ [\![\tilde{w}_i]\!] &= 0 & \text{on } \partial B_{\varepsilon_i}(x_i), \\ [\![q_\varepsilon(\tilde{w}_i)]\!]\cdot n &= k(1-\gamma_i)\varepsilon_i^2 \left(\nabla\tilde{u}_i(x_i)\cdot n + \frac{1}{2}\nabla^3 u_0(x_i) n^3\right) & \text{on } \partial B_{\varepsilon_i}(x_i), \end{cases} \tag{3.17}$$

whose explicit solutions in $\mathbb{R}^2 \setminus \overline{B_{\varepsilon_i}(x_i)}$ are given by

$$\tilde{w}_i(x/\varepsilon) = \varepsilon_i^4 \tilde{g}_i(x) + \varepsilon_i^6 \tilde{h}_i(x), \tag{3.18}$$

where

$$\tilde{g}_i(x) = \frac{\rho_i}{\|x - x_i\|^2} \nabla\tilde{u}_i(x_i)\cdot(x - x_i) \tag{3.19}$$

and

$$\tilde{h}_i(x) = \frac{\rho_i}{2\|x - x_i\|^6} \nabla^3 u_0(x_i)(x - x_i)^3. \tag{3.20}$$

Now, we chose $\tilde{\tilde{u}}_i$ such that it compensates for the discrepancies of order $O(\varepsilon_i^4)$ left on the boundary $\partial\Omega$ by $\tilde{w}_i$ and w_i for $i = 1, \cdots, N$, namely,

$$\begin{cases} \operatorname{div}[q(\tilde{\tilde{u}}_i)] &= 0 & \text{in } \Omega, \\ q(\tilde{\tilde{u}}_i) &= -k\nabla\tilde{\tilde{u}}_i & \text{in } \Omega, \\ q(\tilde{\tilde{u}}_i)\cdot n &= -q(h_i + \tilde{g}_i)\cdot n & \text{on } \partial\Omega, \\ \int_{\Gamma_m} \tilde{\tilde{u}}_i &= -\int_{\Gamma_m} h_i + \tilde{g}_i. \end{cases} \tag{3.21}$$

The boundary layers w_i^j also produce discrepancies on $\partial\Omega$, which are compensated by u_i^j solution of the following boundary value problems for $i, j = 1, \cdots, N$, with $i \neq j$,

$$\begin{cases} \operatorname{div}[q(u_i^j)] &= 0 & \text{in } \Omega, \\ q(u_i^j) &= -k\nabla u_i^j & \text{in } \Omega, \\ q(u_i^j)\cdot n &= -q(\theta_i^j)\cdot n, & \text{on } \partial\Omega, \\ \int_{\Gamma_m} u_i^j &= -\int_{\Gamma_m} \theta_i^j, \end{cases} \tag{3.22}$$

where θ_i^j is given by (3.15).

Finally, the last term of the expansion (3.6), namely $\tilde{\tilde{u}}_\varepsilon$, has to compensate for all remainder terms, so that it is solution to the following boundary value problem

$$\begin{cases} \operatorname{div}[q_\varepsilon(\tilde{\tilde{u}}_\varepsilon)] &= 0 & \text{in } \bigcup_{i=1}^N B_{\varepsilon_i}(x_i) \bigcup \left(\Omega \setminus \bigcup_{i=1}^N \overline{B_{\varepsilon_i}(x_i)}\right), \\ q_\varepsilon(\tilde{\tilde{u}}_\varepsilon) &= -\gamma_\varepsilon k\nabla\tilde{\tilde{u}}_\varepsilon & \text{in } \Omega, \\ q_\varepsilon(\tilde{\tilde{u}}_\varepsilon)\cdot n &= -\sum_{i=1}^N \varepsilon_i^6 q_\varepsilon(\tilde{h}_i)\cdot n & \text{on } \partial\Omega, \\ \int_{\Gamma_m} \tilde{\tilde{u}}_\varepsilon &= -\sum_{i=1}^N \varepsilon_i^6 \int_{\Gamma_m} \tilde{h}_i & \\ [\![\tilde{\tilde{u}}_\varepsilon]\!] &= 0 & \text{on } \bigcup_{i=1}^N \partial B_{\varepsilon_i}(x_i), \\ [\![q_\varepsilon(\tilde{\tilde{u}}_\varepsilon)]\!]\cdot n &= \tilde{\tilde{g}}_\varepsilon & \text{on } \bigcup_{i=1}^N \partial B_{\varepsilon_i}(x_i), \end{cases} \tag{3.23}$$

where,

$$\tilde{\tilde{g}}_\varepsilon = \sum_{i=1}^{N}\sum_{\substack{j=1\\ j\neq i}}^{N} \varepsilon_i^2\varepsilon_j g_{ij}^a + \sum_{i=1}^{N}\varepsilon_i^3 g_i^b + \sum_{i=1}^{N}\varepsilon_i^4(g_i^c + \partial_n h_i) + \sum_{i=1}^{N}\sum_{\substack{j=1\\ j\neq i}}^{N}\varepsilon_i^2\varepsilon_j^2 g_{ij}, \tag{3.24}$$

with

$$g_{ij}^a = (\nabla A_i(\xi_j)n_j)\nabla u_0(x_i)\cdot n_j, \tag{3.25}$$

$$g_i^b = k(1-\gamma_i)\frac{1}{3!}\nabla^4 u_0(\xi_i)n^4, \tag{3.26}$$

$$g_i^c = k(1-\gamma_i)\partial_n\tilde{\tilde{u}}_i, \tag{3.27}$$

$$g_{ij} = k\frac{1-\gamma_j}{\|x-x_j\|^2}A_i(x_j)\nabla u_0(x_i)\cdot(x-x_j), \tag{3.28}$$

for $\xi_j = \delta x + (1-\delta)x_j$, with $\delta\in(0,1)$ and $x\in B_{\varepsilon_j}(x_j)$.

Lemma 3. *Let $\tilde{\tilde{u}}_\varepsilon$ be solution to (3.23) or equivalently solution to the following variational problem: Find $\tilde{\tilde{u}}_\varepsilon\in\mathcal{U}_\varepsilon$, such that*

$$-\int_\Omega q_\varepsilon(\tilde{\tilde{u}}_\varepsilon)\cdot\nabla\eta + \int_{\partial B_\varepsilon}\tilde{\tilde{g}}_\varepsilon\eta - \int_{\partial\Omega}\sum_{i=1}^{N}\varepsilon_i^6 q_\varepsilon(\tilde{h}_i)\cdot n\eta = 0 \quad \forall\eta\in\mathcal{V}, \tag{3.29}$$

where the set $\mathcal{U}_\varepsilon$ and the space $\mathcal{V}$ are defined as

$$\mathcal{U}_\varepsilon := \left\{\varphi\in H^1(\Omega) : \int_{\Gamma_m}\varphi = \sum_{i=1}^{N}\varepsilon_i^6\rho_i\int_{\Gamma_m}\tilde{h}_i\right\} \tag{3.30}$$

and

$$\mathcal{V} := \left\{\varphi\in H^1(\Omega) : \int_{\Gamma_m}\varphi = 0\right\}. \tag{3.31}$$

Then, we have the estimate $\|\tilde{\tilde{u}}_\varepsilon\|_{H^1(\Omega)} = O(|\varepsilon|^5)$ for the remainder, where $|\varepsilon| := max\{\varepsilon_1,\cdots,\varepsilon_N\}$.

Proof. By taking $\eta = \tilde{\tilde{u}}_\varepsilon - \varphi_\varepsilon$ in (3.29), with $\varphi_\varepsilon = \sum_{i=1}^{N}\varepsilon_i^6\rho_i\tilde{h}_i$ on $\partial\Omega$, we have

$$\begin{aligned}-\int_\Omega q_\varepsilon(\tilde{\tilde{u}}_\varepsilon)\cdot\nabla\tilde{\tilde{u}}_\varepsilon + \int_\Omega q_\varepsilon(\tilde{\tilde{u}}_\varepsilon)\cdot\nabla\varphi_\varepsilon + \int_{\partial B_\varepsilon}\tilde{\tilde{g}}_\varepsilon\tilde{\tilde{u}}_\varepsilon - \int_{\partial B_\varepsilon}\tilde{\tilde{g}}_\varepsilon\varphi_\varepsilon \\ - \int_{\partial\Omega}\sum_{i=1}^{N}\varepsilon_i^6 q_\varepsilon(\tilde{h}_i)\cdot n\tilde{\tilde{u}}_\varepsilon + \int_{\partial\Omega}\sum_{i=1}^{N}\varepsilon_i^6 q_\varepsilon(\tilde{h}_i)\cdot n\varphi_\varepsilon = 0\end{aligned} \tag{3.32}$$

Integration by parts yields

$$\begin{aligned}-\int_\Omega q_\varepsilon(\tilde{\tilde{u}}_\varepsilon)\cdot\nabla\tilde{\tilde{u}}_\varepsilon - \int_\Omega \mathrm{div}[q_\varepsilon(\tilde{\tilde{u}}_\varepsilon)]\varphi_\varepsilon + \int_{\partial\Omega} q_\varepsilon(\tilde{\tilde{u}}_\varepsilon)\cdot n\varphi_\varepsilon + \int_{\partial B_\varepsilon}[\![q_\varepsilon(\tilde{\tilde{u}}_\varepsilon)]\!]\cdot n\varphi_\varepsilon \\ + \int_{\partial B_\varepsilon}\tilde{\tilde{g}}_\varepsilon\tilde{\tilde{u}}_\varepsilon - \int_{\partial B_\varepsilon}\tilde{\tilde{g}}_\varepsilon\varphi_\varepsilon - \int_{\partial\Omega}\sum_{i=1}^{N}\varepsilon_i^6 q_\varepsilon(\tilde{h}_i)\cdot n\tilde{\tilde{u}}_\varepsilon + \int_{\partial\Omega}\sum_{i=1}^{N}\varepsilon_i^6 q_\varepsilon(\tilde{h}_i)\cdot n\varphi_\varepsilon = 0.\end{aligned} \tag{3.33}$$

Using equation (3.23), we obtain the equality

$$-\int_\Omega q_\varepsilon(\tilde{\tilde{u}}_\varepsilon)\cdot\nabla\tilde{\tilde{u}}_\varepsilon = \int_{\partial\Omega}\sum_{i=1}^{N}\varepsilon_i^6 q_\varepsilon(\tilde{h}_i)\cdot n\tilde{\tilde{u}}_\varepsilon - \int_{\partial B_\varepsilon}\tilde{\tilde{g}}_\varepsilon\tilde{\tilde{u}}_\varepsilon \tag{3.34}$$

From the Cauchy-Schwarz inequality together with the trace theorem we have

$$\begin{aligned}-\int_\Omega q_\varepsilon(\tilde{\tilde{u}}_\varepsilon)\cdot\nabla\tilde{\tilde{u}}_\varepsilon &\leqslant |\varepsilon|^6\|\tilde{\tilde{u}}_\varepsilon\|_{L^2(\partial\Omega)}\Big\|\sum_{i=1}^{N} q_\varepsilon(\tilde{h}_i)\Big\|_{L^2(\partial\Omega)} + \|\tilde{\tilde{g}}_\varepsilon\|_{H^{\frac{1}{2}}(\partial B_\varepsilon)}\|\tilde{\tilde{u}}_\varepsilon\|_{H^{-\frac{1}{2}}(\partial B_\varepsilon)} \\ &\leqslant C_1|\varepsilon|^6\|\tilde{\tilde{u}}_\varepsilon\|_{H^1(\Omega)} + C_2\|\tilde{\tilde{g}}_\varepsilon\|_{H^1(B_\varepsilon)}\|\tilde{\tilde{u}}_\varepsilon\|_{L^2(B_\varepsilon)}.\end{aligned} \tag{3.35}$$

Now, let us make use of the Hölder inequality together with the Sobolev embedding theorem for $1/p + 1/q$ and $q \geqslant 1$, to obtain

$$\|\tilde{\tilde{u}}_\varepsilon\|_{L^2(B_\varepsilon)} \leqslant C_3|\varepsilon|^{1/q}\|\tilde{\tilde{u}}_\varepsilon\|_{L^{2p}(B_\varepsilon)} \leqslant |\varepsilon|C_4\|\tilde{\tilde{u}}_\varepsilon\|_{H^1(\Omega)}, \tag{3.36}$$

where we have used the interior elliptic regularity of function $\tilde{\tilde{u}}_\varepsilon$. In addition, by using definition (3.24), we obtain

$$\|\tilde{\tilde{g}}_\varepsilon\|_{H^1(B_\varepsilon)} \leqslant C_5|\varepsilon|^4, \tag{3.37}$$

Therefore,

$$-\int_\Omega q_\varepsilon(\tilde{\tilde{u}}_\varepsilon)\cdot\nabla\tilde{\tilde{u}}_\varepsilon \leqslant C_6|\varepsilon|^5\|\tilde{\tilde{u}}_\varepsilon\|_{H^1(\Omega)}. \tag{3.38}$$

Finally, from the coercivity of the bilinear form on the left hand side of the above inequality we obtain

$$c\|\tilde{\tilde{u}}_\varepsilon\|^2_{H^1(\Omega)} \leqslant -\int_\Omega q_\varepsilon(\tilde{\tilde{u}}_\varepsilon)\cdot\nabla\tilde{\tilde{u}}_\varepsilon \leqslant C_6|\varepsilon|^5\|\tilde{\tilde{u}}_\varepsilon\|_{H^1(\Omega)}, \tag{3.39}$$

which leads to the result, namely $\|\tilde{\tilde{u}}_\varepsilon\|_{H^1(\Omega)} \leqslant C|\varepsilon|^5$, with constant $C = C_6/c$ independent of ε. □

3.2. **Asymptotic Expansion of the Shape Functional.** From the ansätz for u_ε given by (3.6), we can obtain the asymptotic expansion of the shape functional $\mathcal{J}_\varepsilon(u_\varepsilon)$ defined through (3.3) with respect to ε. In fact, the shape functional is defined on the boundary Γ_m. Then, let us evaluate the expansion for u_ε on the boundary $\partial\Omega$ to obtain $u_{\varepsilon|\partial\Omega} = (u_0 + \varphi_\varepsilon)_{|\partial\Omega}$, where φ_ε is such that

$$\varphi_\varepsilon = \sum_{i=1}^N \left(\varepsilon_i^2(g_i + \tilde{u}_i) + \varepsilon_i^4(h_i + \tilde{g}_i + \tilde{\tilde{u}}_i) + \varepsilon_i^6\tilde{h}_i\right) + \sum_{i=1}^N\sum_{\substack{j=1\\ j\neq i}}^N \left(\varepsilon_i^2\varepsilon_j^2(\theta_i^j + u_i^j)\right) + \tilde{\tilde{u}}_\varepsilon. \tag{3.40}$$

Therefore,

$$\mathcal{J}_\varepsilon(u_\varepsilon) = \int_{\Gamma_m}(u_0 + \varphi_\varepsilon - U)^2 = \mathcal{J}_0(u_0) + 2\int_{\Gamma_m}(u_0 - U)\varphi_\varepsilon + \int_{\Gamma_m}\varphi_\varepsilon^2. \tag{3.41}$$

Let us now collect the terms on the right-hand side of (3.41) in power of ε. The first one is independent of ε. It is actually the original shape functional. In view of (3.40), the second term can be written as

$$\begin{aligned}\int_{\Gamma_m}(u_0 - U)\varphi_\varepsilon = \sum_{i=1}^N \left(\varepsilon_i^2\int_{\Gamma_m}(u_0 - U)(g_i + \tilde{u}_i) + \varepsilon_i^4\int_{\Gamma_m}(u_0 - U)(h_i + \tilde{g}_i + \tilde{\tilde{u}}_i)\right)\\ + \sum_{i=1}^N\sum_{\substack{j=1\\ j\neq i}}^N \varepsilon_i^2\varepsilon_j^2\int_{\Gamma_m}(u_0 - U)(\theta_i^j + u_i^j) + \sum_{\ell=1}^2 \mathcal{E}_\ell(\varepsilon),\end{aligned} \tag{3.42}$$

where, from the Cauchy-Scharwz inequality together with Lemma 3, we have

$$\mathcal{E}_1(\varepsilon) = \sum_{i=1}^N \varepsilon_i^6\int_{\Gamma_m}(u_0 - U)\tilde{h}_i = O(|\varepsilon|^6), \tag{3.43}$$

$$\mathcal{E}_2(\varepsilon) = \int_{\Gamma_m}(u_0 - U)\tilde{\tilde{u}}_\varepsilon = O(|\varepsilon|^5), \tag{3.44}$$

The last term on the right-hand side of (3.41) can be expanded as follows

$$\int_{\Gamma_m}\varphi_\varepsilon^2 = \int_{\Gamma_m}\Big(\sum_{i=1}^N \varepsilon_i^2(g_i + \tilde{u}_i)\Big)^2 + \sum_{\ell=3}^{15}\mathcal{E}_\ell(\varepsilon), \tag{3.45}$$

with

$$\mathcal{E}_3(\varepsilon) = 2\int_{\Gamma_m}\sum_{i=1}^N \varepsilon_i^2(g_i + \tilde{u}_i)\sum_{i=1}^N \varepsilon_i^4(h_i + \tilde{g}_i + \tilde{\tilde{u}}_i) = O(|\varepsilon|^6), \tag{3.46}$$

$$\mathcal{E}_4(\varepsilon) = 2\int_{\Gamma_m}\Big(\sum_{i=1}^{N}\varepsilon_i^4(h_i+\tilde{g}_i+\tilde{\tilde{u}}_i)\Big)^2 = O(|\varepsilon|^8), \tag{3.47}$$

$$\mathcal{E}_5(\varepsilon) = 2\int_{\Gamma_m}\sum_{i=1}^{N}\sum_{\substack{j=1\\ j\neq i}}^{N}\varepsilon_i^2\varepsilon_j^2(\theta_i^j+u_i^j)\Big(\sum_{i=1}^{N}\varepsilon_i^2(g_i+\tilde{u}_i)\Big) = O(|\varepsilon|^6), \tag{3.48}$$

$$\mathcal{E}_6(\varepsilon) = 2\int_{\Gamma_m}\sum_{i=1}^{N}\sum_{\substack{j=1\\ j\neq i}}^{N}\varepsilon_i^2\varepsilon_j^2(\theta_i^j+u_i^j)\Big(\sum_{i=1}^{N}\varepsilon_i^4(h_i+\tilde{g}_i+\tilde{\tilde{u}}_i)\Big) = O(|\varepsilon|^8), \tag{3.49}$$

$$\mathcal{E}_7(\varepsilon) = \int_{\Gamma_m}\Big(\sum_{i=1}^{N}\sum_{\substack{j=1\\ j\neq i}}^{N}\varepsilon_i^2\varepsilon_j^2(\theta_i^j+u_i^j)\Big)^2 = O(|\varepsilon|^8), \tag{3.50}$$

$$\mathcal{E}_8(\varepsilon) = \int_{\Gamma_m}\sum_{i=1}^{N}\varepsilon_i^6\tilde{h}_i\sum_{i=1}^{N}\varepsilon_i^2(g_i+\tilde{u}_i) = O(|\varepsilon|^8), \tag{3.51}$$

$$\mathcal{E}_9(\varepsilon) = 2\int_{\Gamma_m}\sum_{i=1}^{N}\varepsilon_i^6\tilde{h}_i\sum_{i=1}^{N}\varepsilon_i^4(h_i+\tilde{g}_i+\tilde{\tilde{u}}_i) = O(|\varepsilon|^{10}), \tag{3.52}$$

$$\mathcal{E}_{10}(\varepsilon) = \int_{\Gamma_m}\Big(\sum_{i=1}^{N}\varepsilon_i^6\tilde{h}_i\Big)^2 = O(|\varepsilon|^{12}), \tag{3.53}$$

$$\mathcal{E}_{11}(\varepsilon) = \int_{\Gamma_m}\sum_{i=1}^{N}\varepsilon_i^6\tilde{h}_i\tilde{\tilde{u}}_\varepsilon = O(|\varepsilon|^{11}), \tag{3.54}$$

$$\mathcal{E}_{12}(\varepsilon) = 2\int_{\Gamma_m}\tilde{\tilde{u}}_\varepsilon\sum_{i=1}^{N}\varepsilon_i^2(g_i+\tilde{u}_i) = O(|\varepsilon|^7), \tag{3.55}$$

$$\mathcal{E}_{13}(\varepsilon) = 2\int_{\Gamma_m}\tilde{\tilde{u}}_\varepsilon\sum_{i=1}^{N}\varepsilon_i^4(h_i+\tilde{g}_i+\tilde{\tilde{u}}_i) = O(|\varepsilon|^9), \tag{3.56}$$

$$\mathcal{E}_{14}(\varepsilon) = \int_{\Gamma_m}\tilde{\tilde{u}}_\varepsilon\sum_{i=1}^{N}\varepsilon_i^6\tilde{h}_i = O(|\varepsilon|^{11}), \tag{3.57}$$

$$\mathcal{E}_{15}(\varepsilon) = \int_{\Gamma_m}\tilde{\tilde{u}}_\varepsilon^2 = O(|\varepsilon|^{10}), \tag{3.58}$$

where we have used again the Cauchy-Scharwz inequality together with Lemma 3.

Finally, after replacing (3.42) and (3.45) into (3.41), we obtain the following asymptotic expansion for the topologically perturbed shape functional $\mathcal{J}_\varepsilon(u_\varepsilon)$

$$\begin{aligned}\mathcal{J}_\varepsilon(u_\varepsilon) = \mathcal{J}_0(u_0) &+ 2\sum_{i=1}^{N}\Big(\varepsilon_i^2\int_{\Gamma_m}(u_0-U)(g_i+\tilde{u}_i) + \varepsilon_i^4\int_{\Gamma_m}(u_0-U)(h_i+\tilde{g}_i+\tilde{\tilde{u}}_i)\Big)\\ &+ 2\sum_{i=1}^{N}\sum_{\substack{j=1\\ j\neq i}}^{N}\varepsilon_i^2\varepsilon_j^2\int_{\Gamma_m}(u_0-U)(\theta_i^j+u_i^j) + \int_{\Gamma_m}\Big(\sum_{i=1}^{N}\varepsilon_i^2(g_i+\tilde{u}_i)\Big)^2 + \mathcal{E}(\varepsilon),\end{aligned} \tag{3.59}$$

with

$$\mathcal{E}(\varepsilon) = \sum_{\ell=1}^{15} \mathcal{E}_\ell(\varepsilon) = O(|\varepsilon|^5). \tag{3.60}$$

3.3. **Introduction of Adjoint States.** Note that to evaluate expansion (3.59), we have to solve the problems associated with the non-local terms $\tilde{u}_i$ and $\tilde{\tilde{u}}_i$ for each point x_i, and u_i^j for each pair of points x_i and x_j. However, thanks to the representation we have found, the non-local terms which appears in the first, second and third integrals in (3.59) can be replaced by just one adjoint state independent of the points x_i and x_j. On the other hand, the term $\tilde{u}_i$ also appears in the last integral of expansion (3.59) in a quadratic form, so that $\tilde{u}_i$ has to be computed. Therefore, the adjoint state will be used to replace only the terms involving $\tilde{\tilde{u}}_i$ and u_i^j. In fact, expansion (3.59) can be rewritten as

$$\begin{aligned}
\mathcal{J}_\varepsilon(u_\varepsilon) = \mathcal{J}_0(u_0) &+ 2\sum_{i=1}^{N}\left(\varepsilon_i^2\int_{\Gamma_m}(u_0-U)(g_i+\tilde{u}_i) + \varepsilon_i^4\int_{\Gamma_m}(u_0-U)(h_i+\tilde{g}_i)\right)\\
&+ 2\sum_{i=1}^{N}\left(\varepsilon_i^4\int_{\Gamma_m}(u_0-U)\tilde{\tilde{u}}_i + \sum_{\substack{j=1\\ j\neq i}}^{N}\varepsilon_i^2\varepsilon_j^2\int_{\Gamma_m}(u_0-U)u_i^j\right)\\
&+ 2\sum_{i=1}^{N}\sum_{\substack{j=1\\ j\neq i}}^{N}\left(\varepsilon_i^2\varepsilon_j^2\int_{\Gamma_m}(u_0-U)\theta_i^j\right) + \int_{\Gamma_m}\left(\sum_{i=1}^{N}\varepsilon_i^2(g_i+\tilde{u}_i)\right)^2 + \mathcal{E}(\varepsilon).
\end{aligned} \tag{3.61}$$

Let us introduce an adjoint state solution of the following variational problem: Find $v \in \mathcal{V}$, such that

$$\int_\Omega q(v)\cdot\nabla\eta = 2\int_{\Gamma_m}(u_0-U)\,\eta, \quad \forall \eta \in \mathcal{V}, \tag{3.62}$$

where the space $\mathcal{V}$ is given by (3.31). The associated strong form of (3.62) is written as

$$\left\{\begin{array}{rcll}
\operatorname{div}[q(v)] &=& 0 & \text{in } \Omega,\\
q(v) &=& -k\nabla v, &\\
q(v)\cdot n &=& 2(u_0-U) & \text{on } \Gamma_m,\\
q(v)\cdot n &=& 0 & \text{on } \partial\Omega\setminus\Gamma_m,\\
\int_{\Gamma_m} v &=& 0. &
\end{array}\right. \tag{3.63}$$

The weak form of (3.21) reads: Find $\tilde{\tilde{u}}_i \in \mathcal{U}_i$, such that

$$\int_\Omega q(\tilde{\tilde{u}}_i)\cdot\nabla\eta + \int_{\partial\Omega} q(h_i+\tilde{g}_i)\cdot n\,\eta = 0, \quad \forall\eta\in\mathcal{V}, \tag{3.64}$$

where the space $\mathcal{V}$ is given by (3.31) and the set $\mathcal{U}_i$ is defined as

$$\mathcal{U}_i := \left\{\varphi \in H^1(\Omega) : \int_{\Gamma_m}\varphi = -\int_{\Gamma_m} h_i+\tilde{g}_i\right\}. \tag{3.65}$$

By setting $\eta = \tilde{\tilde{u}}_i + \varphi_i$ as test function in (3.62), with $\varphi_i = h_i + \tilde{g}_i$ on $\partial\Omega$, we obtain the equality

$$\int_\Omega q(v)\cdot\nabla(\tilde{\tilde{u}}_i+\varphi_i) = 2\int_{\Gamma_m}(u_0-U)(\tilde{\tilde{u}}_i+\varphi_i). \tag{3.66}$$

Integration by parts yields

$$\begin{aligned}
\int_\Omega q(v)\cdot\nabla\tilde{\tilde{u}}_i &= 2\int_{\Gamma_m}(u_0-U)\tilde{\tilde{u}}_i + 2\int_{\Gamma_m}(u_0-U)\varphi_i - \int_{\partial\Omega} q(v)\cdot n\varphi_i\\
&= 2\int_{\Gamma_m}(u_0-U)\tilde{\tilde{u}}_i,
\end{aligned} \tag{3.67}$$

since v solves (3.63). Now, let us set $\eta = v$ as test function in (3.64) to obtain the equality

$$\int_\Omega q(\tilde{\tilde{u}}_i)\cdot\nabla v = -\int_{\partial\Omega} q(h_i+\tilde{g}_i)\cdot n\, v. \tag{3.68}$$

After comparing the obtained results we have the following important identity

$$2\int_{\Gamma_m}(u_0-U)\tilde{\tilde{u}}_i = -\int_{\partial\Omega} q(h_i+\tilde{g}_i)\cdot n\, v. \tag{3.69}$$

In addition, the weak form of (3.22) can be written as: Find $u_i^j \in \mathcal{U}_i^j$, such that

$$\int_\Omega q(u_i^j)\cdot\nabla\eta + \int_{\partial\Omega} q(\theta_i^j)\cdot n\,\eta = 0, \quad \forall \eta\in\mathcal{V}, \tag{3.70}$$

with the space $\mathcal{V}$ given by (3.31) and the set $\mathcal{U}_i^j$ given by

$$\mathcal{U}_i^j := \left\{\varphi\in H^1(\Omega); \int_{\Gamma_m}\varphi = -\int_{\Gamma_m}\theta_i^j\right\}. \tag{3.71}$$

After setting $\eta = u_i^j + \varphi_i^j$ as test function in (3.62), with $\varphi_i^j = \theta_i^j$ on $\partial\Omega$, there is

$$\int_\Omega q(v)\cdot\nabla(u_i^j+\varphi_i^j) = 2\int_{\Gamma_m}(u_0-U)(u_i^j+\varphi_i^j). \tag{3.72}$$

From integration by parts we obtain

$$\begin{aligned}\int_\Omega q(v)\cdot\nabla u_i^j &= 2\int_{\Gamma_m}(u_0-U)u_i^j + 2\int_{\Gamma_m}(u_0-U)\varphi_i^j - \int_{\partial\Omega} q(v)\cdot n\varphi_i \\ &= 2\int_{\Gamma_m}(u_0-U)u_i^j,\end{aligned} \tag{3.73}$$

where we have used (3.63). By comparing the last two results, the following important equality holds true

$$2\int_{\Gamma_m}(u_0-U)u_i^j = -\int_{\partial\Omega} q(\theta_i^j)\cdot n\, v. \tag{3.74}$$

Finally, we can respectively replace the third and fourth integrals in (3.61) by the obtained equalities (3.69) and (3.74), namely

$$\begin{aligned}\mathcal{J}(u_\varepsilon) = \mathcal{J}(u_0) &+ 2\sum_{i=1}^N \varepsilon_i^2\int_{\Gamma_m}(u_0-U)(g_i+\tilde{u}_i) \\ &+ \sum_{i=1}^N \varepsilon_i^4\left(2\int_{\Gamma_m}(u_0-U)(h_i+\tilde{g}_i) - \int_{\partial\Omega} q(h_i+\tilde{g}_i)\cdot n\, v\right) \\ &+ \sum_{i=1}^N\sum_{\substack{j=1\\ j\neq i}}^N \varepsilon_i^2\varepsilon_j^2\left(2\int_{\Gamma_m}(u_0-U)\theta_i^j - \int_{\partial\Omega} q(\theta_i^j)\cdot nv\right) + \int_{\Gamma_m}\left(\sum_{i=1}^N \varepsilon_i^2(g_i+\tilde{u}_i)\right)^2 + \mathcal{E}(\varepsilon).\end{aligned} \tag{3.75}$$

Therefore, without any approximation, the integrals in (3.61) involving the non-local terms $\tilde{u}_i$ and u_i^j have been replaced by just one adjoint state v, solution of (3.63), which does not depend on the points x_i and x_j.

4. A non-iterative reconstruction algorithm

In this section we present the resulting non-iterative reconstruction algorithm based on the expansion (3.75). The topological asymptotic expansion of the shape functional $\mathcal{J}(u_\varepsilon)$ given by (3.75) can be rewritten in the following compact form

$$\mathcal{J}(u_\varepsilon) = \mathcal{J}(u_0) + d(\xi)\cdot\alpha + \frac{1}{2}H(\xi)\alpha\cdot\alpha + \mathcal{E}(\varepsilon), \tag{4.1}$$

where $d(\xi)$ and $H(\xi)$ are the first and second order topological derivatives, respectively. In addition, $\alpha = (\varepsilon_1^2,\cdots,\varepsilon_N^2)$ and $\mathcal{E}(\varepsilon)$ is the remainder.

The vector $d(\xi)$ and the matrix $H(\xi)$ are defined as

$$d(\xi) := \begin{pmatrix} d_1 \\ \vdots \\ d_N \end{pmatrix} \qquad \text{and} \qquad H(\xi) := \begin{pmatrix} h_{11} & h_{12} & \cdots & h_{1N} \\ h_{21} & h_{22} & \cdots & h_{2N} \\ \vdots & \vdots & \ddots & \vdots \\ h_{N1} & h_{N2} & \cdots & h_{NN}, \end{pmatrix} \tag{4.2}$$

where each component d_i of the topological derivative vector $d(\xi)$ is given by

$$d_i := b(i) = -2 \int_{\Gamma_m} (u_0 - U)(g_i + \tilde{u}_i) \tag{4.3}$$

while the entries $h_{ij} := A(i,j)$ of the topological Hessian matrix $H(\xi)$ are defined as

$$A(i,i) = 4 \int_{\Gamma_m} (u_0 - U)(h_i + \tilde{g}_i) - 2 \int_{\partial\Omega} (q(h_i + \tilde{g}_i)) \cdot n\, v + 2 \int_{\Gamma_m} (g_i + \tilde{u}_i)^2, \tag{4.4}$$

and, for $i \neq j$,

$$A(i,j) = 2 \int_{\Gamma_m} (u_0 - U)(\theta_i^j + \theta_j^i) - \int_{\partial\Omega} q(\theta_i^j + \theta_j^i) \cdot n\, v + 2 \int_{\Gamma_m} (g_i + \tilde{u}_i)(g_j + \tilde{u}_j). \tag{4.5}$$

In addition, the functions $g_i(x)$, $h_i(x)$, $\tilde{g}_i(x)$ and $\theta_i^j(x)$ are respectively given by (3.10), (3.11), (3.19) and (3.15). Finally, the auxiliary function $\tilde{u}_i$ solves (3.16) and v is solution to the adjoint equation (3.63).

Note that the expression on the right-hand side of (3.75) depends explicitly on the number N of anomalies, their positions xi and sizes α. Thus, let us now introduce the quantity

$$\Psi(\xi, \alpha, N) = d(\xi) \cdot \alpha + \frac{1}{2} H(\xi)\alpha \cdot \alpha. \tag{4.6}$$

After minimizing (4.6) with respect to α we obtain the following linear system

$$\alpha = -(H(\xi))^{-1} d(\xi). \tag{4.7}$$

Let us replace $\alpha = \alpha(\xi)$ solution of (4.7) in (4.6), to obtain

$$\Psi(\xi, \alpha(\xi), N) = -\frac{1}{2} d(\xi) \cdot \alpha(\xi). \tag{4.8}$$

Therefore, the pair of vectors $(\xi^\star, \alpha^\star)$ which minimizes (4.6) is given by

$$\xi^\star := \arg\min_{\xi \in X} \left\{ -\frac{1}{2} d(\xi) \cdot \alpha(\xi) \right\} \quad \text{and} \quad \alpha^\star := \alpha(\xi^\star), \tag{4.9}$$

where X is the set of admissible locations of the inclusions. From these elements the Algorithm 1 is devised. Its input data are given by:

- The number N of anomalies we are going to find;
- The first d and second H order topological derivatives;
- The size of the grid where we are seeking for the anomalies, denoted by n_g;

As a result, the algorithm returns the optimum location and size of the anomalies $(\xi^\star, \alpha^\star)$ for a given number of trial inclusions N, and the associated minimum value of the functional (4.8) denoted as $S^\star$. For more sophisticated approaches based on meta-heuristic and multi-grid methods, we refer to [20]. In Algorithm 1, Π maps the vector of nodal indices $\mathcal{I} = (i_1, i_2, ..., i_N)$ into the corresponding vector of nodal coordinates ξ.

5. Numerical Experiments

Let us apply Algorithm 1 for solving some examples of EIT problem. We consider a disk of unitary radius with center at the origin, namely $\Omega = B_1(0)$. Its electrical conductivity is assumed to be uniform and given by $k = 1$. The boundary of the disk $\partial\Omega$ is subdivided into 16 disjoint pieces representing the electrodes. One pair of such electrodes is selected for injecting and draining the electrical current. Therefore, the excitation Q is given by a pair $Q_{in} = 1$ of injection and $Q_{out} = -1$ of draining. The remainder part of the boundary $\partial\Omega$ remains insulated.

Algorithm 1: Reconstruction Algorithm

Data: N, n_g, d, H
Result: $S^\star$, $\alpha^\star$, $\xi^\star$

Initialization: $S^\star \leftarrow \infty$; $\alpha^\star \leftarrow 0$; $\xi^\star \leftarrow 0$;
for $i_1 \leftarrow 1$ **to** n_g **do**
  for $i_2 \leftarrow i_1 + 1$ **to** n_g **do**
    $\vdots$
    for $i_N \leftarrow i_{N-1} + 1$ **to** n_g **do**
      $$d \leftarrow \begin{pmatrix} b(i_1) \\ b(i_2) \\ \vdots \\ b(i_N) \end{pmatrix}; \quad H \leftarrow \begin{pmatrix} A(i_1,i_1) & A(i_1,i_2) & \cdots & A(i_1,i_N) \\ A(i_2,i_1) & A(i_2,i_2) & \cdots & A(i_2,i_N) \\ \vdots & \vdots & \ddots & \vdots \\ A(i_N,i_1) & A(i_N,i_2) & \cdots & A(i_N,i_N) \end{pmatrix};$$
      $\mathcal{I} \leftarrow (i_1, i_2, \cdots, i_N); \xi \leftarrow \Pi(\mathcal{I}); \alpha \leftarrow -H^{-1}d$;
      if $\alpha_k > 0 \quad \forall k \in \{1, \ldots, N\}$ **then**
        $S \leftarrow -\frac{1}{2} d \cdot \alpha$;
        if $S < S^\star$ **then**
          $S^\star \leftarrow S$;
          $\alpha^\star \leftarrow \alpha$;
          $\xi^\star \leftarrow \xi$;
        end if
      end if
    end for
  end for
end for
return $S^\star$, $\alpha^\star$, $\xi^\star$

The associated potential U is measured on the whole $\Gamma_m = \partial\Omega$ or on a part $\Gamma_m \subsetneq \partial\Omega$ of the boundary of the disk. For more than one measurement, this procedure is repeated by changing the selected pair of injection and draining electrodes. From these information we are going to reconstruct an unknown number of anomalies with contrast $\gamma_i = 2$, for $i = 1, \cdots, N^*$. See sketch in Figure 4.

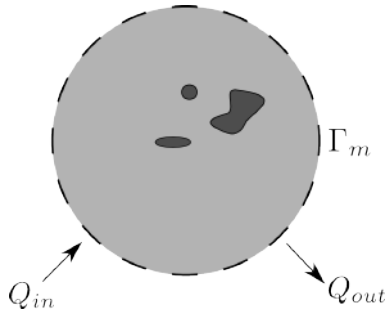

FIGURE 4. Model problem.

The auxiliary boundary value problems are solved using a finite element mesh with 32768 elements and 16641 nodes. From these solutions the sensitivities can be numerically evaluated at any point of the mesh. However, because of the high complexity of Algorithm 1 [20], a sub-mesh is defined over the finite element mesh where the combinatorial search is performed, leading to the optimal solution $(\alpha^\star, \xi^\star)$ defined in the sub-mesh.

In the case of noisy data, the electrical conductivity k^* is corrupted with White Gaussian Noise (WGN) of zero mean and standard deviation μ. Therefore, k^* is replaced by $k^*_\mu = k^*(1 + \mu\,\nu)$, where ν is a function assuming random values in the interval $(-1, 1)$ and μ corresponds to the noise level.

5.1. **Complete Boundary Measurements.** In this section we present five examples concerning total boundary measurements ($\Gamma_m = \partial\Omega$). The first example shows the sensitivity of the reconstruction with respect to the size of the sub-mesh. In the second example we propose a non-iterative procedure to find the unknown number of anomalies. In the third example a L-shaped anomaly is approximated by a number of trial balls. Finally, in the fourth and fifth examples the robustness of the reconstruction method with respect to noisy data is investigated.

5.1.1. *Example 1: Sensitivity of the reconstruction with respect to the size of the sub-mesh.* In this case, the sensitivity of the method with respect to the size of the sub-mesh is studied. We consider three sub-meshes, namely, the first one with 81 interior nodes, the second one with 289, and the third sub-mesh with 1089 interior nodes. The target ω^* consists of a ball-shaped anomaly with radius $\varepsilon^* = 0.15$ and center at $x^* = (0.4431, 0.313)$. One boundary measurement is used in the reconstruction process.

We start with a sub-mesh of 81 trial points. Then it is uniformly refined twice, leading respectively to 289 and 1089 trial points. The results associated with each discretization are respectively shown in Figures 5(a), 5(b) and 5(c). From an inspection of the results presented Figure 5, we observe that the more the sub-mesh is refined the better is the reconstruction. In particular, if the center of the target does not belongs to the set of nodes of the sub-mesh, namely $x^* \notin X$, the algorithm returns a location $x^\star$ which is the closest to x^*, as shown in Figures 5(a) and 5(b). Finally, when $x^* \in X$, the algorithm returns the exact location, as can be seen in Figure 5(c). In all cases, each resulting size $\varepsilon^\star$ is very close to the actual one ε^*. For a quantitative analysis of the results obtained, see the convergence curves for $\|x^\star - x^*\|$ and $|\varepsilon^\star - \varepsilon^*|$ in Figure 6.

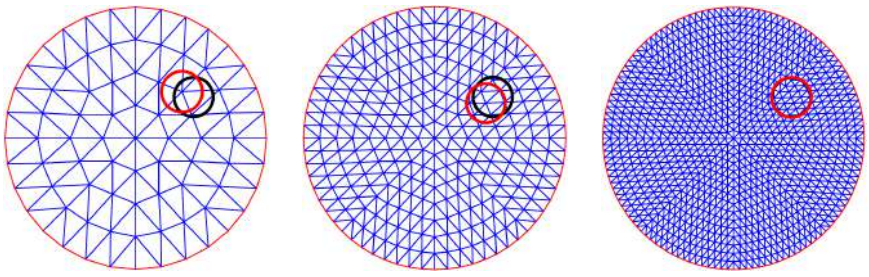

(a) 81 trial points (b) 289 trial points (c) 1089 trial points

FIGURE 5. Example 1: Results obtained for different sub-meshes. The red and black circles represent the solution and the target, respectively.

In order to show different features of the reconstruction Algorithm 1, from now on we assume that the center of each anomaly to be reconstructed coincides with one point of the sub-mesh, which has 289 points.

5.1.2. *Example 2: Seeking for the number of anomalies.* In this example the target consists of three anomalies with different sizes, as showed in Figure 7 and Table 1. We use three boundary measurements in the reconstruction process.

We start the reconstruction algorithm by taking $N = 1$ and proceed to increasing the value of N until that the vector of optimal sizes $\alpha^\star$ contains one entry with negligible value. The results are shown in Figure 8. For $N = 1$ and $N = 2$ the solutions are clearly far from the target. For $N = 3$ the locations are perfectly reconstructed and the sizes are very close to the target. Finally, for $N = 4$ there is an additional anomaly with negligible size, namely $\varepsilon^\star_4 \approx 8.4556 \times 10^{-3}$. Therefore we can conclude that the correct quantity of anomalies is $N^\star = 3$. Note that this

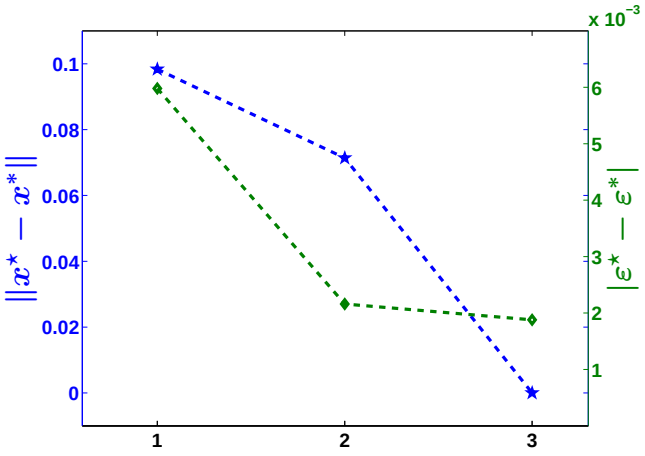

FIGURE 6. Example 1: Convergence curves for $\|x^\star - x^*\|$ and $|\varepsilon^\star - \varepsilon^*|$.

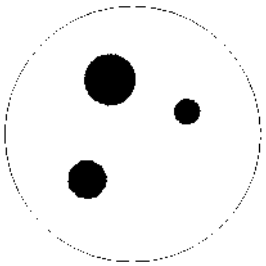

FIGURE 7. Example 2: Target with three anomalies.

TABLE 1. Example 2: Locations and sizes of the target anomalies.

	ω_1^*	ω_2^*	ω_3^*
x^*	(-0.1768,0.4268)	(-0.3536,-0.3536)	(0.4268,0.1768)
ε^*	0.2	0.15	0.1

procedure is not iterative, since there is no relation between the results for two consecutive values of N. In addition, we can start the Algorithm 1 based on the assumption that there exists $N > N^*$ and find a number $(N - N^\star)$ of trial balls with negligible sizes in just one shot. The quantitative results are presented in the Table 2. Note that in all cases the total volume and center of mass of the set of anomalies are almost preserved.

TABLE 2. Example 2: Results obtained for different number N of trial balls.

		$N = 1$	$N = 2$	$N = 3$	$N = 4$
$\omega_1^\star$	$x_1^\star$	(-0.1768,0.1768)	(-0.0884,0.3384)	(-0.1768,0.4268)	(-0.1768,0.4268)
	$\varepsilon_1^\star$	0.2575	0.2283	0.2029	0.1976
$\omega_2^\star$	$x_2^\star$		(-0.3536,-0.3536)	(-0.3536,-0.3536)	(-0.3536,-0.3536)
	$\varepsilon_2^\star$		0.1373	0.1448	0.1454
$\omega_3^\star$	$x_3^\star$			(0.4268,0.1768)	(0.4268,0.1768)
	$\varepsilon_3^\star$			0.0965	0.0997
$\omega_4^\star$	$x_4^\star$				(-0.3681,0.6387)
	$\varepsilon_4^\star$				8.4556×10^{-3}

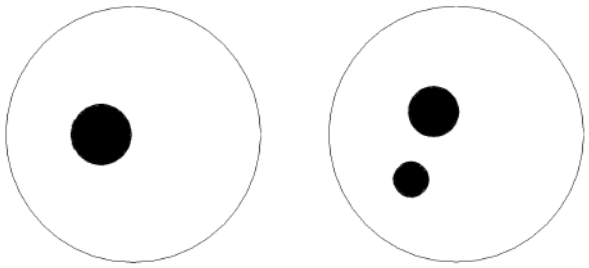

(a) $N = 1$ (b) $N = 2$

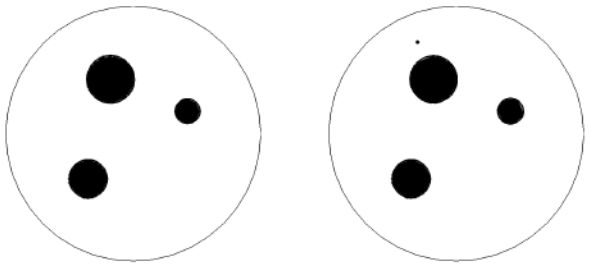

(c) $N = 3$ (d) $N = 4$

FIGURE 8. Experiment 2: Results obtained for different number N of trial balls.

5.1.3. *Example 3: Simultaneous topology and shape reconstruction.* In this example the topology as well as the shape of the anomalies are reconstructed. The target shown in Figure 9 consists of a ball and a L-shaped anomalies. The number of trial balls is set as $N = 4$. The obtained results for different number M of boundary measurements are shown in Figure 10. For $M = 2$ the reconstruction shown in Figure 10(a) is poor, whereas for $M = 4$, $M = 8$ and $M = 16$ the reconstructions can be considered quite good, as respectively shown in Figures 10(b), 10(c) and 10(d).

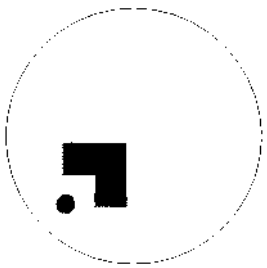

FIGURE 9. Example 3: Target with a ball and a L-shaped anomalies.

5.1.4. *Example 4: Reconstruction from noisy data.* Now we are interested in investigating the robustness of the method with respect to noisy data. The target consists of four anomalies of same sizes, as shown in Figure 11 and Table 3. The electrical conductivity k^* is corrupted with a noise of level $\mu = 10\%$.

TABLE 3. Example 4: Location and sizes of the target anomalies.

	ω_1^*	ω_2^*	ω_3^*	ω_4^*
x^*	(0.4268,0.1768)	(-0.3536,0.4268)	(-0.1768,-0.1768)	(0.3681,-0.6387)
ε^*	0.1	0.1	0.1	0.1

The obtained results for different number M of boundary measurements are shown in Figure 12. For $M = 2$ the reconstruction fails, as shown in Figure 12(a), whereas for $M = 4$, $M = 8$

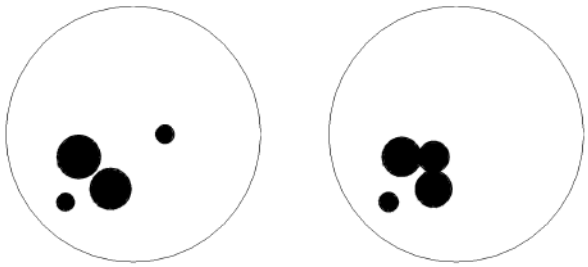

(a) $M = 2$ (b) $M = 4$

(c) $M = 8$ (d) $M = 16$

FIGURE 10. Example 3: Results obtained for different numbers M of complete boundary measurements.

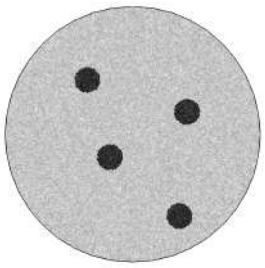

FIGURE 11. Example 4: Target corrupted with $\mu = 10\%$ of White Gaussian Noise.

and $M = 16$ the reconstructions are quite good, as shown in Figures 12(b), 12(c) and 12(d). The quantitative results are presented in Table 4.

TABLE 4. Example 4: Solutions for different values of M and with $\mu = 10\%$ of White Gaussian Noise.

		$M = 2$	$M = 4$	$M = 8$	$M = 16$
$\omega_1^\star$	$x_1^\star$	(0.3536,0.3536)	(-0.3536,0.3536)	(0.3681,-0.6387)	(-0.1768,-0.1768)
	$\varepsilon_1^\star$	0.0993	0.1025	0.0958	0.0919
$\omega_2^\star$	$x_2^\star$	(-0.3536,0.3536)	(0.0000,-0.2500)	(0.4268,0.1768)	(0.3681,-0.6387)
	$\varepsilon_2^\star$	0.1016	0.0920	0.0917	0.0981
$\omega_3^\star$	$x_3^\star$	(0.0000,-0.2500)	(0.3681,-0.6387)	(-0.0884,-0.2134)	(0.4268,0.1768)
	$\varepsilon_3^\star$	0.0925	0.0919	0.0898	0.0865
$\omega_4^\star$	$x_4^\star$	(0.3681,-0.6387)	(0.4268,0.1768)	(-0.2652,0.3902)	(-0.1768,0.4268)
	$\varepsilon_4^\star$	0.0953	0.0944	0.1055	0.1055

5.1.5. *Example 5: Increasing the noise level.* Let us test again the robustness of the method with respect noisy data. The target is the same as before, namely, it consists of four anomalies as shown in Figure 11 and Table 3. The electrical conductivity is now corrupted with different levels

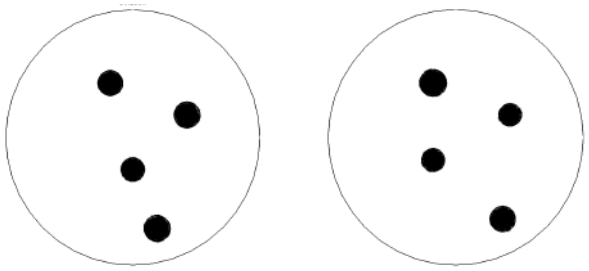

(a) $M = 2$ (b) $M = 4$

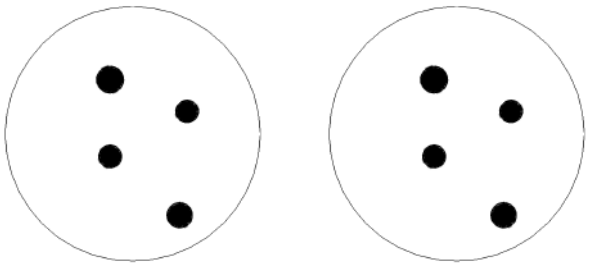

(c) $M = 8$ (d) $M = 16$

FIGURE 12. Example 4: Solutions for different values of M and with $\mu = 10\%$ of White Gaussian Noise.

of noise, which are given by $\mu = 10\%, \mu = 15\%$ and $\mu = 20\%$, as shown in Figures 13(a), 14(a) and 15(a), respectively. The reconstructions obtained with $M = 64$ boundary measurements are shown in Figures 13(b), 14(b) and 15(b) for $\mu = 10\%, \mu = 15\%$ and $\mu = 20\%$, respectively. The quantitative results are presented in Table 5.

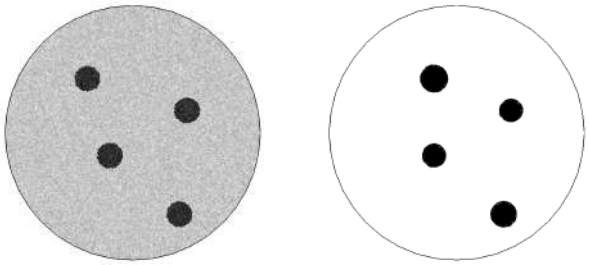

(a) $\mu = 10\%$ (b) $M = 64$

FIGURE 13. Example 5: Target corrupted with $\mu = 10\%$ of White Gaussian Noise (left) and obtained result with $M = 64$ complete boundary measurements (right).

5.2. **Partial Boundary Measurements.** In this last example we consider partial boundary measurements $\Gamma_m \subsetneq \partial\Omega$. More precisely, the electric potential are measured on the regions representing the electrodes. See thick lines in Figure 4.

5.2.1. *Example 6: Partial boundary measurements with noisy data.* The target consists of three ball-shaped anomalies, which is corrupted with different levels of noise $\mu = 10\%, \mu = 15\%$ and $\mu = 20\%$, as described in Table 6 and shown in Figures 16(a), 17(a) and 18(a), respectively. The reconstructions obtained with $M = 64$ boundary measurements are shown in Figures 16(b), 17(b) and 18(b). The quantitative results are presented in Table 7.

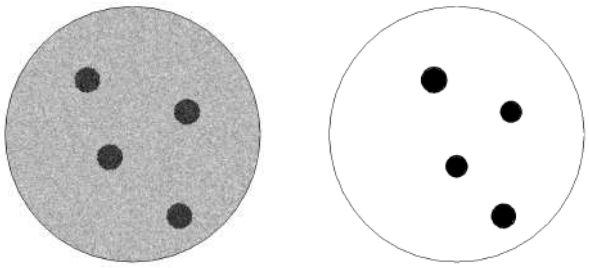

(a) $\mu = 15\%$ (b) $M = 64$

FIGURE 14. Example 5: Target corrupted with $\mu = 15\%$ of White Gaussian Noise (left) and obtained result with $M = 64$ complete boundary measurements (right).

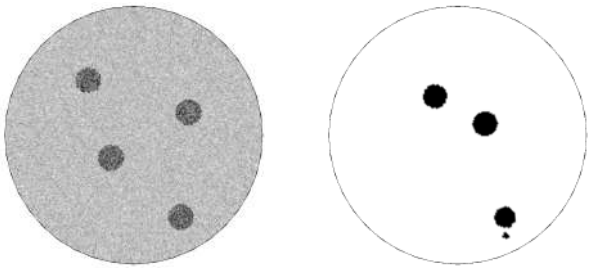

(a) $\mu = 20\%$ (b) $M = 64$

FIGURE 15. Example 5: Target corrupted with $\mu = 20\%$ of White Gaussian Noise (left) and obtained result with $M = 64$ complete boundary measurements (right).

TABLE 5. Example 5: Solutions for different values of μ and $M = 64$ complete boundary measurements.

		$\mu = 10\%$	$\mu = 15\%$	$\mu = 20\%$
$\omega_1^\star$	$x_1^\star$	(-0.3536,0.3536)	(0.3681,-0.6387)	(0.3681,-0.6387)
	$\varepsilon_1^\star$	0.1009	0.0929	0.0824
$\omega_2^\star$	$x_2^\star$	(-0.1768,-0.1768)	(0.0000,-0.1250)	(0.3754,-0.7813)
	$\varepsilon_2^\star$	0.0823	0.0914	0.0240
$\omega_3^\star$	$x_3^\star$	(0.3681,-0.6387)	(0.3902,0.2652)	(0.2134,0.0884)
	$\varepsilon_3^\star$	0.0981	0.0772	0.0956
$\omega_4^\star$	$x_4^\star$	(0.4268,0.1768)	(-0.2652,0.3902)	(-0.1768,0.3018)
	$\varepsilon_4^\star$	0.0984	0.0935	0.0916

TABLE 6. Example 6: Location and sizes of the target anomalies.

	ω_1^*	ω_2^*	ω_3^*
x^*	(0.4268,0.1768)	(-0.3536,-0.3536)	(-0.1768,0.4268)
ε^*	0.1	0.1	0.1

6. CONCLUDING REMARKS

In this paper a new reconstruction method for a class of electrical impedance tomography problems has been proposed. It relies on the topological derivatives concept. The basic idea consists in rewrite the inverse problem as a topology optimization problem, where a shape

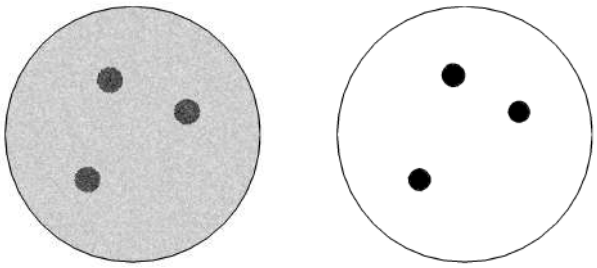

(a) (b)

FIGURE 16. Target corrupted with $\mu = 10\%$ of White Gaussian Noise (left) and obtained result with $M = 64$ partial boundary measurements (right).

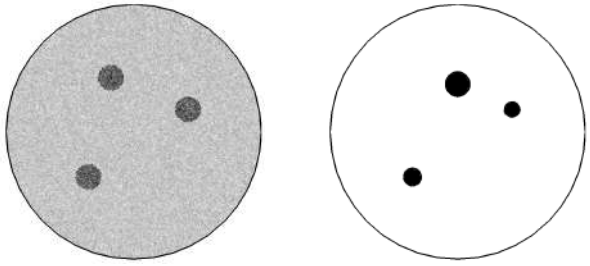

(a) (b)

FIGURE 17. Target corrupted with $\mu = 15\%$ of White Gaussian Noise (left) and obtained result with $M = 64$ partial boundary measurements (right).

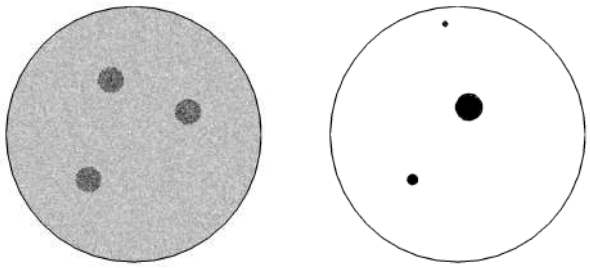

(a) (b)

FIGURE 18. Target corrupted with $\mu = 20\%$ of White Gaussian Noise (left) and obtained result with $M = 64$ partial boundary measurements (right).

TABLE 7. Example 6: Solutions for different values of μ and $M = 64$ partial boundary measurements.

		$\mu = 10\%$	$\mu = 15\%$	$\mu = 20\%$
$\omega_1^\star$	$x_1^\star$	(0.4268,0.1768)	(0.3902,0.2652)	(0.0884,0.2134)
	$\varepsilon_1^\star$	0.0804	0.0795	0.1022
$\omega_2^\star$	$x_2^\star$	(-0.3536,-0.3536)	(-0.3536,-0.3536)	(-0.3536,-0.3536)
	$\varepsilon_2^\star$	0.0827	0.0771	0.0396
$\omega_3^\star$	$x_3^\star$	(-0.0884,0.4634)	(-0.0884,0.3384)	(-0.0975,0.8654)
	$\varepsilon_3^\star$	0.0870	0.1007	0.0181

functional measuring the misfit between the boundary measurements and the electrical potentials obtained from the model has been minimized with respect to a set of ball-shaped anomalies of different sizes. The adjoint method has been evoked *a posteriori*, after obtaining the associated sensitivities, allowing us to derive a simpler representation for the resulting expansion, which has been truncated up to the second order term, leading to a quadratic and strictly convex form with respect to the volume of the inclusions. Therefore, the truncated expansion has been used to devise a novel non-iterative reconstruction algorithm based on a simple optimization step. As a result, the reconstruction process has become very robust with respect to noisy data and also independent of any initial guess. Finally, some numerical experiments taking into account total and partial boundary measurements have been presented, showing different features of the proposed reconstruction algorithm. Since the proposed method can approximate accurately the unknown set of hidden anomalies by several balls, it can be used for supplying a good initial guess for more complex iterative approaches such as the ones based on level-sets methods, for instance.

Acknowledgements

This research was partly supported by CNPq (Brazilian Research Council), CAPES (Brazilian Higher Education Staff Training Agency) and FAPERJ (Research Foundation of the State of Rio de Janeiro). These supports are gratefully acknowledged.

References

[1] G.S. Alberti, H. Ammari, B. Jin, J.-K. Seo, and W. Zhang. The linearized inverse problem in multifrequency electrical impedance tomography. *To appear on the SIAM Journal on Imaging Sciences*, 9:1525–1551, 2016.

[2] H. Ammari, J. Garnier, W. Jing, H. Kang, M. Lim, K. Sølna, and H. Wang. *Mathematical and statistical methods for multistatic imaging*, volume 2098. Springer, 2013.

[3] H. Ammari, J. Garnier, V. Jugnon, and H. Kang. Stability and resolution analysis for a topological derivative based imaging functional. *SIAM Journal on Control and Optimization*, 50(1):48–76, 2012.

[4] H. Ammari and H. Kang. *Reconstruction of small inhomogeneities from boundary measurements*. Lectures Notes in Mathematics vol. 1846. Springer-Verlag, Berlin, 2004.

[5] H. Ammari and G. Uhlmann. Reconstruction of the potential from partial Cauchy data for the Schrodinger equation. *Indiana University Mathematics Journal*, 53(1):169–183, 2004.

[6] E. Beretta, Y. Capdeboscq, F. G., and E. Francini. Thin cylindrical conductivity inclusions in a three-dimensional domain: a polarization tensor and unique determination from boundary data. *Inverse Problems*, 25(6):065004, 2009.

[7] M. Bonnet. Higher-order topological sensitivity for 2-D potential problems. *International Journal of Solids and Structures*, 46(11–12):2275–2292, 2009.

[8] A.P. Calderón. On an inverse boundary value problem. *Computational and Applied Mathematics*, 25(2-3), 2006. Reprinted from the Seminar on Numerical Analysis and its Applications to Continuum Physics, Sociedade Brasileira de Matemática, Rio de Janeiro, 1980.

[9] A. Canelas, A. Laurain, and A. A. Novotny. A new reconstruction method for the inverse source problem from partial boundary measurements. *Inverse Problems*, 31(7):075009, 2015.

[10] Y. Capdeboscq and M. S. Vogelius. A general representation formula for boundary voltage perturbations caused by internal conductivity inhomogeneities of low volume fraction. *Mathematical Modelling and Numerical Analysis*, 37(1):159–173, 2003.

[11] D. J. Cedio-Fengya, S. Moskow, and M. S. Vogelius. Identification of conductivity imperfections of small diameter by boundary measurements. Continuous dependence and computational reconstruction. *Inverse Problems*, 14(3):553–595, 1998.

[12] A. Friedman and M. Vogelius. Identification of small inhomogeneities of extreme conductivity by boundary measurements: a theorem on continuous dependence. *Archive for Rational Mechanics and Analysis*, 105(4):299–326, 1989.

[13] M. Hintermüller, A. Laurain, and A. A. Novotny. Second-order topological expansion for electrical impedance tomography. *Advances in Computational Mathematics*, 36(2):235–265, 2012.

[14] A. M. Il'in. *Matching of asymptotic expansions of solutions of boundary value problems*. Translations of Mathematical Monographs, vol. 102. American Mathematical Society, Providence, RI, 1992.

[15] V. Isakov, S. Leung, and J. Qian. A fast local level set method for inverse gravimetry. *Communications in Computational Physics*, 10(4):1044–1070, 2011.

[16] R. Kohn and M. Vogelius. Identification of an unknow conductivity by means of measurements at the boundary. *Inverse Problems*, 14:113–123, 1984.

[17] R. Kohn and M. Vogelius. Relaxation of a variational method for impedance computed tomography. *Communication on Pure and Applied Mathematics*, 40(6):745–777, 1987.

[18] R V Kohn, H Shen, M S Vogelius, and M I Weinstein. Cloaking via change of variables in electric impedance tomography. *Inverse Problems*, 24(1):015016, 2008.

[19] A. Leitão and J. Baumeister. *Topics in Inverse Problems*. IMPA Mathematical Publications, Rio de Janeiro, 2005.

[20] T. J. Machado, J. S. Angelo, and A. A. Novotny. A new one-shot pointwise source reconstruction method. *Mathematical Methods in the Applied Sciences*, DOI: 10.1002/mma.4059, 2016.

[21] W. G. Mazja, S. A. Nasarow, and B. A. Plamenewski. *Asymptotics of solutions to elliptic boundary-value problems under a singular perturbation of the domain*. Tbilisi University, Tbilisi, 1981. (in Russian).

[22] V. G. Maz'ya, S. A. Nazarov, and B. A. Plamenevskij. *Asymptotische theorie elliptischer randwertaufgaben in singulär gestörten gebieten, vol. 1*. Akademie-Verlag, Berlin, 1991. (English transl.: Asymptotic theory of elliptic boundary value problems in singularly perturbed domains, vol. 1, Basel: Birkhäuser Verlag, 2000).

[23] V. G. Maz'ya, S. A. Nazarov, and B. A. Plamenevskij. *Asymptotic theory of elliptic boundary value problems in singularly perturbed domains. Vol. I*, volume 111 of *Operator Theory: Advances and Applications*. Birkhäuser Verlag, Basel, 2000. Translated from the German by Georg Heinig and Christian Posthoff.

[24] S. A. Nazarov. *Asymptotic expansions of eigenvalues*. Leningrad University, Leningrad, 1987.

[25] S. A. Nazarov and B. A. Plamenevskij. *Elliptic problems in domains with piecewise smooth boundaries*, volume 13 of *de Gruyter Expositions in Mathematics*. Walter de Gruyter & Co., Berlin, 1994.

[26] A. A. Novotny and J. Sokołowski. *Topological derivatives in shape optimization*. Interaction of Mechanics and Mathematics. Springer-Verlag, Berlin, Heidelberg, 2013.

Laboratório Nacional de Computação Científica LNCC/MCT, Coordenação de Matemática Aplicada e Computacional, Av. Getúlio Vargas 333, 25651-075 Petrópolis - RJ, Brasil

E-mail address: andreydf@lncc.br,novotny@lncc.br